Role of Mg ions in modulating the morphology and structure of $CaCO_3$ crystals grown in aqueous foams†

Debabrata Rautaray, Manasi Kasture and Murali Sastry*

Received 27th January 2005, Accepted 13th July 2005
First published as an Advance Article on the web 18th July 2005
DOI: 10.1039/b501420b

We investigate the role of magnesium ions in modulating the morphology and crystallography of $CaCO_3$ crystals grown in aqueous foam. This is accomplished by first making foams from an aqueous mixture of $CaCl_2$ + $MgCl_2$ and the anionic surfactant aerosol-OT (AOT) followed by reaction of the foam with Na_2CO_3 solution. The Ca^{2+} and Mg^{2+} ions electrostatically complex with AOT and react with Na_2CO_3 within the foam to yield $CaCO_3$ crystals of interesting morphology. These studies indicate that $CaCO_3$ in a fractured, needle-like morphology was formed at high Mg^{2+} concentrations in the foam whereas porous, rhombic $CaCO_3$ crystals were obtained at low Mg^{2+} concentrations. The effect of water drainage time and thereby, the structure of the foam on the morphology of the $CaCO_3$ crystals grown was also studied.

Introduction

Many living organisms contain biominerals and composites with finely tuned properties, reflecting a remarkable degree of control over nucleation, growth and shape of the constituent crystals.[1] Such morphologically complex, 3-D structures if produced synthetically, could find important applications as lightweight ceramics, catalyst supports, biomedical implants, hybrid materials and cosmetic formulations.[2] Recognizing that the most complex and exquisite mineral crystallization occurs in biological systems, various biomimetic templates such as Langmuir monolayers,[3–5] self-assembled monolayers (SAMs),[6,7] the liquid–liquid interface,[8–10] functionalized polymer surfaces[11,12] and lipid bilayer stacks[13] have been investigated and show great promise in crystal engineering. An essential objective of biomimetic materials science is to develop new synthetic strategies capable of synthesizing materials and composites that exhibit organizational and multifunctional specificity.[14]

Calcium carbonate is an important biomineral that has found wide application in ion exchange processes due to its strong surface interactions with heavy metals in the environment.[15] Many impurity ions are found to affect $CaCO_3$ crystal growth. The effect of incorporating foreign ions such as Cd, Sr,[15] Cu, Mn,[16] Fe,[15,17] Co,[18] Li,[19,20] Mg[15,21–27] and organic matter[24,25,28] into $CaCO_3$ crystals has been studied in great detail. In particular, Mg^{2+} has been studied extensively as an additive,[15,21–27] mainly because Mg^{2+} ions are found in biological environments in high concentrations and are believed to play a critical role in $CaCO_3$ formation in nature.[29] Incorporation of magnesium within biological $CaCO_3$ is widespread, with many containing magnesium of different levels of concentrations leading to control over both the precipitation of calcite and aragonite depending on the extent of magnesium inclusion within the crystals.[26]

Aqueous foams are a mixture of a gas (in the form of bubbles) and water stabilized by a surfactant. The foam lamellae in aqueous foams offer the possibility of binding various charged metal ions with surfactants at the gas–liquid interface and has been demonstrated in this laboratory to be an excellent medium for growing a wide variety of inorganic materials.[30–36] Previous reports on foam-based synthesis of various nanomaterials include metal nanoparticles such as gold[30] and silver,[31] magnetic nanomaterials such as Co, Ni and their subsequent conversion into Co–Ag and Co–Ni core shell nanoparticles, respectively,[32,33] and minerals such as calcium carbonate[34,35] and iron oxyhydroxide.[36] The synthesis of $CaCO_3$ crystals in an aqueous foam involves first the formation of aerosol OT (AOT)-stabilized foams using an aqueous solution of $CaCl_2$ followed by reaction of the foam with Na_2CO_3, this process resulting in the formation of calcite spheroaggregates.[35] We further exploit this novel procedure for mineral growth and investigate the role of crystal growth inhibitors such as Mg ions on the morphology of $CaCO_3$ crystals synthesized in an aqueous foam. The crucial step in our foam-based method for the synthesis of inorganic materials is the complexation of metal ions with the surfactant in water before creation of the foam by nitrogen gas bubbling. Recognizing that competition of additives such as Mg^{2+} ions in solution with Ca^{2+} ions for electrostatic binding with AOT would determine the composition of the foam (*i.e.*, molar ratio of Ca^{2+}:Mg^{2+}) and consequently the effect of the additive on crystal morphology, we have studied the strength of interaction of calcium and magnesium cations with AOT molecules by isothermal titration calorimetry (ITC). ITC is an extremely powerful thermodynamic technique that has been used with much success in understanding biomolecular binding

---

Nanoscience Group, Materials Chemistry Division, National Chemical Laboratory, Pune – 411 008, India. E-mail: sastry@ems.ncl.res.in; Fax: +91 20 25893952/25893044; Tel: + 91 20 25893044

† Electronic supplementary information (ESI) available: Isothermal titration calorimetric data recorded during successive injections of 10 µl aqueous $CaCl_2$ (A) and $MgCl_2$ (B) solution (10^{-2} M) into the titration cell containing 1.47 ml of water (C and D). Binding isotherms obtained by integration of the raw data are shown in (A) and (B) plotted as a function of total volume of metal ion solution injected. See http://dx.doi.org/10.1039/b501420b

processes.[37–41] It is widely used in biochemistry to study protein–ligand,[37] protein–protein,[38] DNA–RNA,[39] DNA–protein[40] and protein–lipid[41] interactions. In spite of its well-demonstrated ability to study the thermodynamics of chemical reactions, ITC has remained relatively under-exploited in inorganic materials synthesis. As a first step in applying ITC to inorganic materials synthesis, we have recently employed ITC to study the binding of amino acids[42] and DNA–PNA[43] with gold nanoparticles.

In this paper, we investigate the growth of $CaCO_3$ crystals in foams with different concentrations of the additive, Mg^{2+}. This is accomplished by generating foams from an aqueous mixture of $CaCl_2$ + $MgCl_2$ + AOT followed by reaction with Na_2CO_3 solution. We investigate the role of magnesium ions for two different Ca^{2+}:Mg^{2+} molar ratios in directing morphology control and polymorph selectivity in $CaCO_3$ crystallization. These studies show the formation of $CaCO_3$ in a fractured needle-like morphology at the higher Mg ion concentration in the foam whereas porous, rhombic $CaCO_3$ crystals were obtained at the lower Mg ion concentration. Since the thickness of the liquid lamellae in the foam can be controlled by the amount of water drainage within the plateau borders of the foam, we also show that the morphology of the resulting inorganic crystals may be controlled *via* the time of drainage of the foam. Presented below are details of our study.

Experimental

In a typical experiment, a rectangular column of 50 cm height and a square base of 10 × 10 cm^2 with sintered ceramic discs embedded in it were used for generation of the foam. An aqueous mixture of 100 ml of AOT (10^{-2} M) + $CaCl_2$ (10^{-2} M) + $MgCl_2$ (10^{-3} M) was taken in the rectangular column and the foam built up by injecting air at a pressure of 1–5 psig through the ceramic disc. Stable foams of 40 cm height could be routinely obtained. The liquid lamellae between bubbles in the foam may be considered to consist of two Langmuir monolayers of AOT complexed electrostatically with metal cations and therefore amenable to reaction with carbonate anions at the interface. After stabilization of the foam, the aqueous AOT + $CaCl_2$ + $MgCl_2$ solution was carefully drained out from below and the foam subjected to a mild and fine spray of aqueous solution of 10^{-2} M (100 ml) sodium carbonate. The foam collapsed gradually (typically 15 to 20 min after spraying of Na_2CO_3) and the crystals of calcium carbonate were collected through the outlet provided at the bottom of the column. Experiments were performed at Ca^{2+}:Mg^{2+} molar ratios of 10:1 (AOT (10^{-2} M) + $CaCl_2$ (10^{-2} M) + $MgCl_2$ (10^{-3} M) and 100:1 (AOT (10^{-2} M) + $CaCl_2$ (10^{-2} M) + $MgCl_2$ (10^{-4} M).

In order to understand the process of formation of $CaCO_3$ crystals, their growth was effected in the foam as described above at two different times of drainage of the foam. This was done by carrying out reaction of the AOT + $CaCl_2$ + $MgCl_2$ foam with Na_2CO_3 solution after allowing 10 min and 5 h for drainage of the liquid from the AOT + $CaCl_2$ + $MgCl_2$ foam. The process of drainage of the water in the foam is expected to lead to variation in the thickness of the water channels in the foam.

Scanning electron microscopy (SEM) and energy dispersive analysis of X-rays (EDAX) measurements of drop-cast films of the $CaCO_3$ crystals grown deposited on Si (111) substrates were carried out on a Leica Stereoscan-440 SEM equipped with a Phoenix EDAX attachment. Samples for transmission electron microscopy (TEM) analysis were prepared by drop-coating films of the $CaCO_3$ crystals on carbon-coated copper TEM grids, allowing the grid to stand for 2 min after which the extra solution was removed using a blotting paper. TEM analysis was performed on a JEOL model 1200EX instrument operated at an accelerating voltage at 120 kV. X-ray diffraction (XRD) analysis of drop-cast films of the $CaCO_3$ crystals deposited on glass substrates was carried out on a Phillips PW 1830 instrument operating at a voltage of 40 kV and a current of 30 mA with Cu Kα radiation. Fourier transform infrared spectroscopy (FTIR) measurements of drop-cast films of the $CaCO_3$ crystals deposited on Si (111) substrates were carried out in the diffuse reflectance mode at a resolution of 2 cm^{-1} on a Perkin Elmer FTIR – Spectrum One instrument. Contact angle measurements of drop-cast films of $CaCO_3$ crystals on silicon substrates were carried out by the sessile water-drop method (1 μl water drop) using a Rame-Hart 100 goniometer.

Isothermal titration calorimetric (ITC) measurements were carried out to characterize the interaction between aqueous AOT solutions with calcium and magnesium ions. The calorimeter consists of two cells: a reference cell filled with pure solvent (water) and a sample titration cell filled with 1.47 ml of aqueous AOT solution (10^{-3} M). In two separate experiments, 10^{-2} M aqueous solutions of $CaCl_2$ and $MgCl_2$ were added separately from the syringe into the titration cell containing aqueous AOT solution in small steps of 10 μl (30 injections). The heat evolved/absorbed during reaction of calcium and magnesium ions with AOT solution were measured, the time between successive injections of aqueous solutions of $CaCl_2$ and $MgCl_2$ being 2 min. ITC measurements were carried out using a MicroCal VP-ITC instrument at 300 K.

Results and discussion

Fig. 1A and B show representative SEM images at different magnifications of $CaCO_3$ crystals synthesized by treating AOT + $CaCl_2$ + $MgCl_2$ (Ca:Mg = 10:1) foam with Na_2CO_3 solution after allowing drainage of liquid from the foam for 5 h. Fig. 1A shows highly dense needle-shaped $CaCO_3$ crystals populating the substrate surface. At higher magnification, the $CaCO_3$ needles are observed to have regular and uniform fractures on their surface. The width of the $CaCO_3$ needles are calculated to be in the range of 50–100 nm while the lengths are in excess of 2–5 μm. The cracks on the $CaCO_3$ needles are typically in the range of 10–20 nm in width. EDAX measurement from the needle-shaped crystals shown in Fig. 1A and B yielded strong Ca, C and O signals together with signals of Mg, Na, S and Cl (curve 1 in Fig. 2A). The EDAX spectrum after the formation of $CaCO_3$ clearly shows the presence of Mg ions (used as an impurity ion) as well as Na and S due to the surfactant, AOT. The presence of the Cl signal is possibly due to the $CaCl_2$ and $MgCl_2$ salts used as precursors in the initial reaction. The Ca:Mg atomic ratios in the $CaCO_3$ crystals in this and subsequent experiments have been determined by atomic

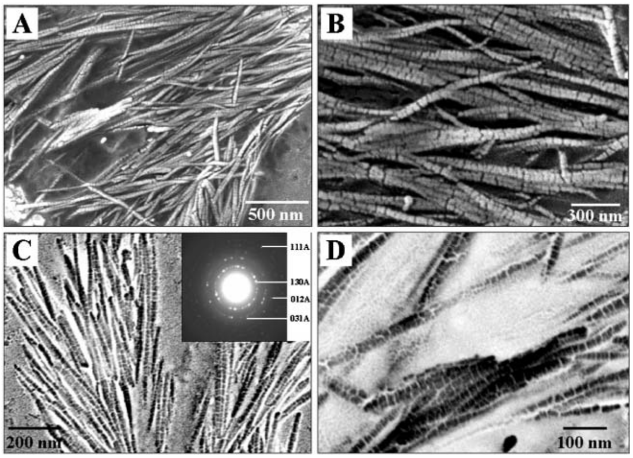

Fig. 1 Low and high magnification SEM images (A and B) and TEM images (C and D) of $CaCO_3$ crystals synthesized by treating AOT + $CaCl_2$ + $MgCl_2$ (Ca:Mg = 10:1) foam with Na_2CO_3 solution after allowing the foam to drain for 5 h. The inset in C shows the selected area electron diffraction pattern recorded from the crystals shown in the main part of the figure. The electron diffraction rings are indexed in the figure where 'A' stands for aragonite.

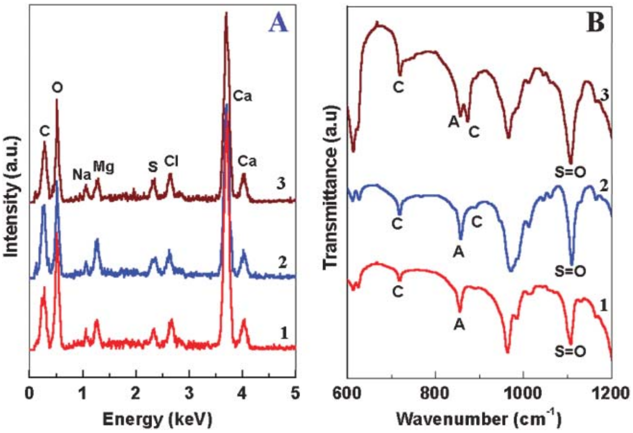

Fig. 2 (A) EDAX profiles recorded from $CaCO_3$ crystals synthesized by treating AOT + $CaCl_2$ + $MgCl_2$ (Ca:Mg molar ratio = 10:1) foam with Na_2CO_3 solution after allowing the foam to drain for 5 h (curve 1) and the AOT + $CaCl_2$ + $MgCl_2$ (Ca:Mg molar ratio = 100:1) foam following reaction with Na_2CO_3 solution after allowing the foam to drain for 5 h (curve 2) and 10 min (curve 3). (B) FTIR spectra recorded from $CaCO_3$ crystals synthesized by treating AOT + $CaCl_2$ + $MgCl_2$ (Ca:Mg molar ratio = 10:1) foam with Na_2CO_3 solution after allowing the foam to drain for 5 h (curve 1) and AOT + $CaCl_2$ + $MgCl_2$ (Ca:Mg molar ratio = 100:1) foam after reaction with Na_2CO_3 solution after allowing the foam to drain for 5 h (curve 2) and 10 min (curve 3); 'A' stands for aragonite and 'C' stands for calcite.

absorption spectroscopy (AAS) measurements, to be discussed later. AAS is a more sensitive method for estimation of such ratios than EDAX.

Representative TEM images at different magnifications from the calcium carbonate crystals synthesized by using foam with a Ca:Mg in a molar ratio of 10:1 after allowing drainage of liquid from the foam for 5 h are shown in Fig. 1C and D. The TEM images of the $CaCO_3$ crystals also clearly support the fractured nature of the needles observed in the SEM images (Fig. 1A and B). Apparently, the high magnification TEM image (Fig. 1D) was unable to resolve the individual crystallites of $CaCO_3$ constituting the individual needles. An estimate of the thickness of the individual cracks on the needles was made from the TEM image to be *ca*. 10–20 nm, consistent with the SEM results. The inset of Fig. 1C shows the selected area electron diffraction (SAED) pattern of the calcium carbonate crystals shown in Fig. 1C. The diffraction rings have been indexed in the figure based on the aragonite polymorph of $CaCO_3$.[44]

FTIR measurement of the needle-shaped $CaCO_3$ crystals (curve 1 in Fig. 2B) exhibited prominent absorption bands at 717, 857 and 1105 cm^{-1}. The strong absorption band at 857 cm^{-1} is characteristic of the aragonite polymorph of $CaCO_3$.[45,46] The weak absorption band at 717 cm^{-1} is attributed to calcite and is clearly present along with the aragonite phase in this synthesis. The characteristic IR absorption peak of aragonite that is normally observed at 855 cm^{-1} is seen to shift to 857 cm^{-1} while that of the calcite phase shifts from 712 to 717 cm^{-1}. The shift to longer wavenumbers of the aragonite and calcite absorption bands are due to Mg^{2+} substitution in the $CaCO_3$ lattice which causes increased structural disorder.[26,27] The characteristic IR absorption peak of the S=O stretching vibration of the sulfonate group present in the AOT molecules shifts from 1057 to 1105 cm^{-1} clearly indicating electrostatic complexation of Ca^{2+} ions with the sulfonate groups of AOT.[47] The XRD pattern recorded from the needle-shaped $CaCO_3$ crystals cast in the form of a film on a glass substrate (curve 1 in Fig. 3) shows a number of Bragg reflections characteristic of the aragonite (indicated by 'A')[44] polymorph along with a small percentage of calcite (indicated by 'C').[44] Please note that the peak at 44° arises from the sample holder of the instrument. The broadening in the Bragg reflections in the XRD data (Fig. 3, curve 1) is thus in agreement with the extremely small size of the $CaCO_3$ crystals inferred from the SEM and TEM images (Fig. 1). The XRD, SAED and FTIR results thus

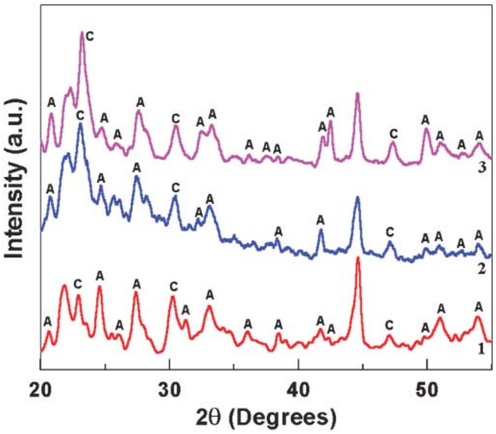

Fig. 3 XRD patterns recorded from $CaCO_3$ crystals grown by treating AOT + $CaCl_2$ + $MgCl_2$ (Ca:Mg = 10:1) foam with Na_2CO_3 solution after allowing the foam to drain for 5 h (curve 1) and AOT + $CaCl_2$ + $MgCl_2$ (Ca:Mg = 100:1) foam after reaction with Na_2CO_3 solution after allowing the foam to drain for 5 h (curve 2) and 10 min (curve 3). (A – stands for aragonite and C – stands for calcite).

conclusively show that the needle-shaped $CaCO_3$ crystals are nano-crystalline in nature and are predominantly of the aragonite polymorph. Contact angle measurements of a sessile water drop at different points on the surface of drop-cast films of the $CaCO_3$ crystals yielded an average value of 87°. The needle-shaped $CaCO_3$ crystals are thus quite hydrophobic and most likely are enveloped by AOT molecules. The crystallization of $CaCO_3$ was also achieved by treating the AOT + $CaCl_2$ + $MgCl_2$ (Ca:Mg = 10:1) foam with Na_2CO_3 solution but with a drainage of liquid from the foam for only 10 min (to obtain a wet foam). Even with smaller drainage times, we did not observe any discernible change in the nature of the fractured needle-shaped aragonite crystals (data not shown). It is clear from the above that the presence of Mg ions in the foam lamellae is responsible for the shape and polymorph control of $CaCO_3$ crystals with minimal contribution of the water content in the foam lamellae.

The effect of magnesium ion concentration on the morphology and crystallography of $CaCO_3$ crystals was also studied in the foam template. Experiments were performed with a starting Ca:Mg molar ratio of 100:1 with drainage periods of 5 h (dry foam) and 10 min (wet foam). Fig. 4A and B show SEM images at different magnifications of $CaCO_3$ crystals grown in the foam by treating AOT + $CaCl_2$ + $MgCl_2$ (Ca:Mg molar ratio = 100:1) foam with Na_2CO_3 solution after allowing drainage of liquid from the foam for 5 h. At low magnification (Fig. 4A), a number of rhombic $CaCO_3$ crystals are observed, which are highly porous in nature. The higher magnification SEM image (Fig. 4B) clearly shows the rhombic $CaCO_3$ crystals to be composed of a number of defects in the central part and on the edges of the crystals. EDAX analysis of the porous $CaCO_3$ crystals yielded Ca, C and O signals along with Mg, Na, S and Cl signals as well (curve 2 in Fig. 2A). The EDAX spectrum clearly shows the presence of Mg in this case with Na and S components from AOT (curve 2 in Fig. 2A). The porous nature of the rhombic $CaCO_3$ crystals is very prominently seen in the lower magnification TEM image shown in Fig. 4C. The high magnification TEM image reveals that $CaCO_3$ crystals are mesoporous in nature (Fig. 4D) with the pores of dimensions in the range 0.1–0.8 μm. The TEM image in the inset of Fig. 4D shows the mesoporous nature of the $CaCO_3$ crystals in greater detail. The fringes (Kikuchi fringes) in this image underline the crystalline nature of the fibrous crystals in the mesoporous $CaCO_3$ structure. The inset of Fig. 4C shows the SAED pattern recorded from the mesoporous calcium carbonate crystals. The SAED pattern obtained is characteristic of a highly crystalline phase and has been indexed in this case based on the calcite polymorph of $CaCO_3$.[44] FTIR measurement from the rhombic $CaCO_3$ porous plates is shown as curve 2 in Fig. 2B. This curve exhibits a strong absorption band at 856 cm^{-1} indicating the formation of aragonite in this case as well with an increase in intensity of the absorption band for calcite at 713 cm^{-1}. A weak absorption band due to calcite at 875 cm^{-1} arose in this case indicating the formation of a mixed phase of $CaCO_3$.[45,46] The shifted S=O stretching vibration at 1105 cm^{-1} in the FTIR spectrum indicates the presence of AOT molecules in the $CaCO_3$ crystals formed. The XRD data provides clear support to the FTIR measurement showing the formation of a mixed phase of aragonite and calcite polymorphs (curve 2 in Fig. 3). The XRD peaks are relatively broad in this case as well indicating that the porous $CaCO_3$ crystals are indeed made up of much smaller crystallites. Contact angle measurements of the rhombic $CaCO_3$ porous crystals yielded an average value of 91°. The $CaCO_3$ crystals thus obtained in this case are hydrophobic in nature due to AOT molecules surrounding the crystallites.

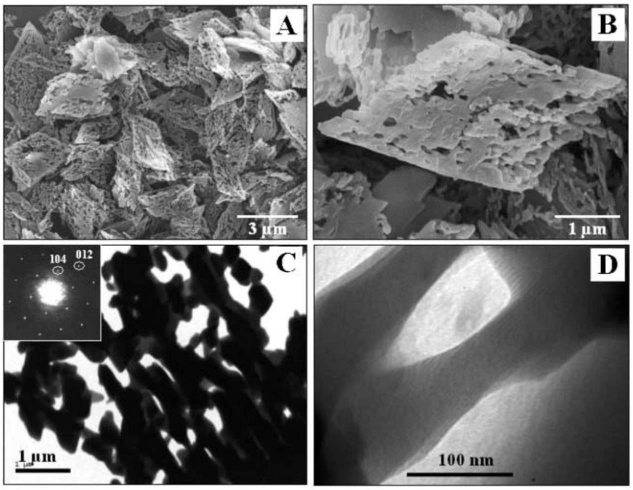

Fig. 4 Low and high magnification SEM images (A and B) and TEM images (C and D) of $CaCO_3$ crystals synthesized by treating AOT + $CaCl_2$ + $MgCl_2$ (Ca:Mg = 100:1) foam with Na_2CO_3 solution after allowing the foam to drain for 5 h. The inset in C shows the selected area electron diffraction pattern recorded from the crystals shown in the main part of the figure. The electron diffraction spots corresponding to calcite are indexed in the figure. The inset in D shows a particular mesoporous region of the main figure in greater detail. The scale bar in the inset of D corresponds to 50 nm.

The crystallization of $CaCO_3$ was also achieved by treating AOT + $CaCl_2$ + $MgCl_2$ (Ca:Mg molar ratio = 100:1) foam with Na_2CO_3 solution but with a lower drainage time (10 min) of liquid from the foam. It may be noted that the thickness of the plateau borders and the dimensions of the plateau junctions is known to change as a function of time of drainage of the foam. Fig. 5A and B show SEM images at different magnifications of $CaCO_3$ crystals grown in this experiment. At low magnification (Fig. 5A), a number of rhombic $CaCO_3$ crystals are observed in this case as well but with a much reduced porosity of the crystal surface [compare with the high drainage time (5 h) experiment (Fig. 4A)]. The high magnification SEM image (Fig. 5B) further underlines this inference. EDAX analysis of the $CaCO_3$ crystals shown in Fig. 5A and B yielded Ca, C and O signals along with Mg, Na, S and Cl signals (curve 3 in Fig. 2A). The EDAX spectrum thus clearly shows the presence of Mg ions in this case as well with Na and S arising from AOT (curve 3 in Fig. 2A). TEM images (Fig. 5C and D) recorded from the edges of the solid rhombic $CaCO_3$ crystals show the mesoporous nature of the crystals in this case even though the crystal porosity is much reduced. The inset of Fig. 5D shows the SAED pattern of the mesoporous calcium carbonate crystals. The SAED pattern obtained has been indexed in the figure based on the calcite polymorph of $CaCO_3$.[44] FTIR measurement from the solid

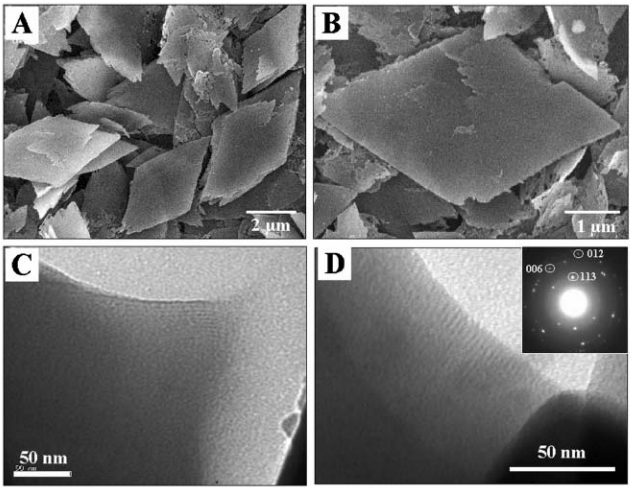

Fig. 5 Low and high magnification SEM images (A and B) and TEM images (C and D) of $CaCO_3$ crystals synthesized by treating AOT + $CaCl_2$ + $MgCl_2$ (Ca:Mg molar ratio = 100:1) foam with Na_2CO_3 solution after allowing the foam to drain for 10 min. The inset in D shows the selected area electron diffraction pattern recorded from the crystals shown in the main part of the figure. The electron diffraction pattern has been indexed based on the calcite structure of the crystals.

rhombic $CaCO_3$ plates is shown as curve 3 in Fig. 2B and exhibited strong absorption bands at 713 and 875 cm^{-1} indicating the formation of calcite with a weak absorption band corresponding to aragonite at 856 cm^{-1}. As in all previous experiments, the presence of a shifted S=O (1105 cm^{-1}) stretching vibration attests to the presence of AOT molecules on the surface of the crystals. The XRD data provides clear support to the FTIR measurements showing the formation of a mixed phase of the aragonite and calcite polymorphs with an increase in calcite Bragg reflection intensities (curve 3 in Fig. 3). Contact angle measurements from the $CaCO_3$ crystals formed in this case yielded an average value of 89°. The $CaCO_3$ crystals thus obtained in this case are hydrophobic in nature as well due to AOT molecules surrounding the crystallites.

We would like to mention here that the morphology of the $CaCO_3$ crystals grown in the presence of Mg ions in AOT foam are very different from previous reports on $CaCO_3$ crystal growth in the presence of impurity ions.[15–27] In earlier studies on synthetic and biological magnesian calcites, it was proposed that magnesium could be located at interstitial sites, dislocations or on the crystal surface. However, incorporation of magnesium ions within biological calcites is widespread. It is commonly known that biological systems mostly control the precipitation of calcite rather than aragonite.[26] The incorporation of Mg ions in aquatic biomineralized calcites is perhaps an unavoidable consequence of the crystallization environments that invariably contain Mg ions.

Support for the important role played by the Mg ions in the AOT foam is provided by various control experiments wherein (i) $CaCO_3$ crystals were grown in solution by the reaction of $CaCl_2$ and Na_2CO_3 in the presence of AOT; (ii) $CaCO_3$ crystals were grown in a foam formed by bubbling air in an aqueous mixture of $CaCl_2$ and AOT and allowing the foam to drain for 10 min, where $CaCO_3$ growth was induced by reaction with Na_2CO_3 solution; and (iii) $CaCO_3$ crystals grown in a AOT + $CaCl_2$ + $MgCl_2$ mixed solution with Ca^{2+}/Mg^{2+} in a molar ratio of 10:1 and 100:1 after reacting with Na_2CO_3.

The $CaCO_3$ crystals grown in solution by the reaction of $CaCl_2$ and Na_2CO_3 in the presence of AOT yielded large, rhombohedral calcite crystals assembled into a rudimentary close-packed structure (Fig. 6A) with no resemblance to the $CaCO_3$ structures observed in the foam lamellae containing Mg ions. $CaCO_3$ crystals grown in the foam in the absence of Mg ions resulted in the formation of calcite spheroaggregates (Fig. 6B), consistent with our earlier observations.[35] The $CaCO_3$ crystals grown in solution by the reaction of $CaCl_2$ and Na_2CO_3 in the presence of AOT at a Ca:Mg molar ratio of 10:1 resulted in the formation of a mixture of fibrous as well as rhombohedral $CaCO_3$ crystals (Fig. 6C), indicating the formation of a mixed phase of aragonite and calcite (determined from FTIR and XRD measurements; data not shown) while the reaction carried out at a Ca:Mg molar ratio of 100:1 yielded stacks of calcite plates (Fig. 6D). We note that in these latter control experiments, the morphology of the $CaCO_3$ is completely different from those synthesized in the foam lamellae in the presence of Mg ions (Fig. 1 and 4).

In order to understand the strength and nature of interaction of calcium and magnesium ions with AOT molecules, isothermal titration calorimetric (ITC) measurements were performed. Fig. 7A shows the ITC titration data recorded during injection of 10 µl of aqueous $CaCl_2$ (10^{-2} M) from a syringe into 1.47 ml of aqueous AOT (10^{-3} M) solution taken in the sample cell. It is seen from the figure that the reaction is exothermic, where each peak is the result of a single injection. The exothermicity of the first few injections is roughly the same since during the initial stages of reaction between Ca^{2+} and AOT molecules, a number of binding sites are available for complexation. As the injections progress, the number of

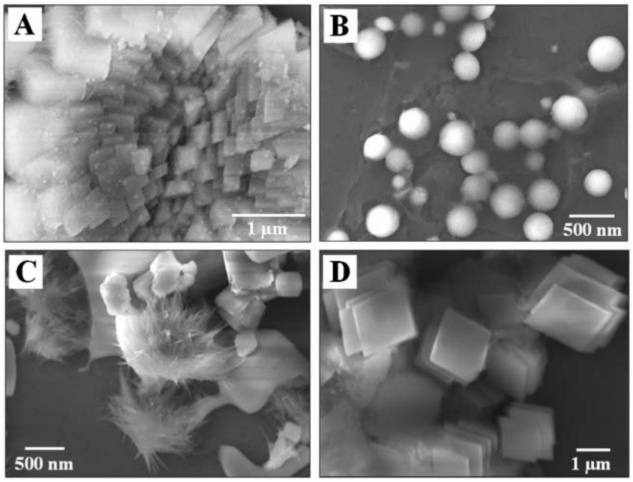

Fig. 6 SEM images of $CaCO_3$ crystals synthesized in various control experiments. SEM image of $CaCO_3$ crystals grown in solution by the reaction of $CaCl_2$ and Na_2CO_3 in the presence of AOT (A); $CaCO_3$ crystals grown in a foam formed by bubbling air in an aqueous mixture of $CaCl_2$ and AOT and allowing the foam to drain for 10 min followed by reaction with Na_2CO_3 solution (B); $CaCO_3$ crystals grown by reacting Na_2CO_3 with AOT + $CaCl_2$ + $MgCl_2$ mixed solution with a Ca^{2+}/Mg^{2+} molar ratio of 10:1 (C) and 100:1 (D).

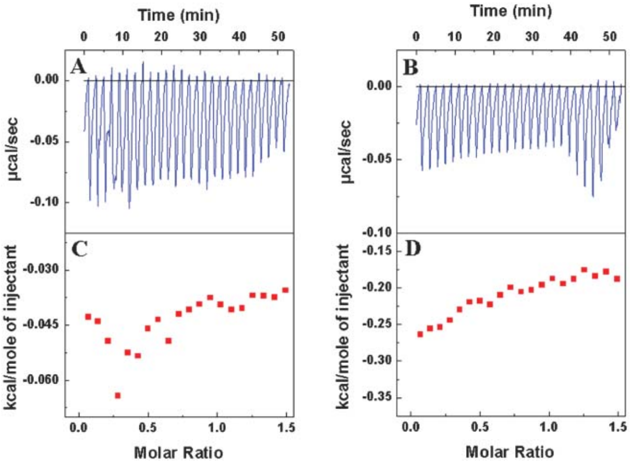

Fig. 7 (A and B) Isothermal titration calorimetric data recorded during successive injections of 10 µl aqueous $CaCl_2$ (A) and $MgCl_2$ (B) solution (10^{-2} M) into the titration cell containing 1.47 ml of aqueous AOT solution (10^{-3} M). (C & D) Binding isotherms obtained by integration of the raw data shown in the A and B, respectively, plotted as a function of the AOT:metal ion molar ratio in solution.

binding sites decreases continuously and is tracked by a monotonic drop in exothermicity of the reaction (Fig. 7A). In the case of the $MgCl_2$-AOT ITC measurement, a similar calorimetric response is observed (Fig. 7B). The plots shown in Fig. 7C and D are the binding isotherms determined from the raw data, where the total heat per injection (in kcal per mole of $CaCl_2$ and $MgCl_2$ injected, respectively) is plotted against the AOT:metal ion molar ratio in solution in the titration cell. Please note that the calorimetric response measured during dilution of the salt solutions in water has been subtracted from the data obtained during reaction of the different metal ions with AOT (supporting information, Fig. S1)† and has been shown after this correction in Fig. 7. From the binding isotherms in Fig. 7C and D, we note that the exothermicity of reaction of Mg^{2+} ions with AOT is considerably higher than that recorded from Ca^{2+} ions indicating much stronger interaction of Mg ions with this surfactant. Such differences in binding of metal ions with AOT would be expected to influence the molar ratio of Ca:Mg ions in the foam and is expected to be rather different than the molar ratio of ions present in solution.

The ITC results provide information on the preferential binding of metal ions with the surfactant. The amount of metal ion uptake in the foam was estimated by a chemical analysis of the foam by atomic absorption spectroscopy (AAS). The $CaCO_3$ crystals formed in the foam at different Mg ion concentrations were subjected to AAS measurements to estimate the amount of the metal ions present in the foam and compared with the ratio of the metal ions present in the starting solution. AAS analysis of the AOT + $CaCl_2$ + $MgCl_2$ foam was carried out after spraying of Na_2CO_3 for $CaCO_3$ crystallization. AAS measurement of the parent solutions from which the foams were built yielded Ca:Mg ratios of 9:1 (in the Ca:Mg = 10:1 experiment) and 89:1 (in the Ca:Mg = 100:1 experiment) while the corresponding ratios for the foam after reaction with Na_2CO_3 and formation of the crystals was of 5:1 (Ca:Mg = 10:1 experiment) and 33:1 (Ca:Mg = 100:1 experiment), respectively. The increase in concentration of Mg ions in the $CaCO_3$ crystals in both cases relative to the parent solutions clearly indicates stronger binding of Mg ions with AOT than Ca ions and is thus consistent with the stronger interaction of Mg ions with AOT relative to Ca ions determined by ITC measurements (Fig. 7).

A thorough understanding of the $CaCO_3$–Mg system requires an accurate assessment of the extent to which Mg^{2+} modifies $CaCO_3$ solubility. We believe that small concentrations of additives typically affect crystallization *via* adsorption of the active ions at a number of growth sites on the surface of pre-critical nuclei, which consequently prevents their growth. Incorporation of small amounts of inhibitors into a crystallite may also create internal strain, thus increasing the solubility and the critical size required for a stable precipitate. Mg^{2+} ions can affect crystal morphologies by both Mg^{2+} adsorption on specific crystal faces and by altering the crystal nucleation and growth processes. As briefly described above, organisms use Mg^{2+} ions as well as organic macromolecules to control $CaCO_3$ precipitation.[26,29] They have mechanisms for effectively dehydrating Mg^{2+} ions, which may also promote Mg-incorporation within calcite nuclei.[26,29] The presence of Mg ions causes considerable changes in the morphology of $CaCO_3$ crystals, which may be important in the construction of architecturally complex structures produced by organisms for specific purposes.

The plateau borders in the foam provide spaces of anisotropic confinement to the solution trapped in these regions bounded by charged templates for immobilizing charged species such as metal ions. Comparatively, the plateau junctions encompass a greater volume of solution and are more isotropic in spatial extent. The thickness of both the plateau borders and the plateau junctions decreases with increasing time of drainage as the foam dries. As seen in the SEM and TEM images (Fig. 1), the fine needles of $CaCO_3$ are most likely synthesized in the plateau border regions reflecting its narrow confinement. During treatment of the foam with Na_2CO_3 solution, we believe that even though the hydrodynamic flow of the liquid through the foam by capillary action drives the calcite needles to the more capacious plateau junctions, they do not aggregate into bigger structures at the junction as high Mg^{2+} content stabilizes them, whereas with a lower Mg^{2+} content porous rhombic calcite plates are observed, which are bigger in size and are possibly synthesized in the plateau junction. The porous nature of calcite plates is due to the presence of Mg ions inducing defects in the $CaCO_3$ lattice planes. It is also possible that the metastable phase (aragonite) forms first and may subsequently recrystallize into magnesian calcite. At a lower time of drainage (10 min), the plateau borders and junctions contain greater amount of entrapped water. Under these conditions, the formation of rhombic $CaCO_3$ crystals is observed with no sign of porosity, because of the high water content. It is expected that at a lower drainage time, more Ca^{2+} ions are present in the foam lamellae along with water that would be available for secondary growth on the porous calcite crystals leading to the formation of more compact solid surface. Though we believe this to be the mechanism and is thus at this time speculative, studies are under progress to establish and understand in detail the microstructure of the foam lamellae and the dynamics involved in it.

In conclusion, we have investigated the role of magnesium ions in controlling the morphology and polymorphism of $CaCO_3$ in liquid foams. Our studies reveal that $CaCO_3$ in a fractured needle-like morphology is obtained with a higher Mg^{2+} content in the aqueous foam whereas porous rhombic $CaCO_3$ crystals are observed at lower Mg^{2+} concentrations. A combination of interfacial templating area provided by the liquid lamellae in foams stabilized by ionizable surfactants and the dynamic nature of the foam bubbles makes this method potentially exciting for the controlled synthesis of inorganic materials.

Acknowledgements

D.R. thanks the Department of Science and Technology (DST), Govt. of India for a research fellowship. This work was partially sponsored by a grant from the Council of Scientific and Industrial Research (P23CMM0022), Government of India, and is gratefully acknowledged. We thank Ms Ragini Hariharan for assistance in some of the experimental work and Mr Pravin S. Shirude, Organic Chemistry (Synthesis) Division, for assistance with the ITC measurements.

References

1 C. A. Orme, A. Noy, A. Wierzbicki, M. T. McBride, M. Grantham, H. H. Teng, P. M. Dove and J. J. DeYoreo, *Nature*, 2001, **14**, 775–779.
2 E. Matijevic, *Curr. Opin. Colloid Interface Sci.*, 1996, **1**, 176.
3 B. R. Heywood and S. Mann, *Langmuir*, 1992, **8**, 1492.
4 E. Loste, E. Diaz-Marti, A. Zarbakhsh and F. C. Meldrum, *Langmuir*, 2003, **19**, 2830.
5 D. Rautaray, S. R. Sainkar, N. R. Pavaskar and M. Sastry, *CrystEngComm*, 2002, **4**, 626.
6 J. Kuther, G. Nelles, R. Seshadri, M. Schaub, H. J. Butt and W. Tremel, *Chem. Eur. J.*, 1998, **4**, 1834.
7 J. Aizenberg, A. J. Black and G. M. Whitesides, *J. Am. Chem. Soc.*, 1999, **121**, 4500.
8 D. Rautaray, A. Kumar, S. Reddy, S. R. Sainkar, N. R. Pawaskar and M. Sastry, *CrystEngComm*, 2001, 45.
9 D. Rautaray, A. Banpurkar, S. R. Sainkar, A. V. Limaye, S. Ogale and M. Sastry, *Cryst. Growth Des.*, 2003, **3**, 449.
10 D. Rautaray, A. Banpurkar, S. R. Sainkar, A. V. Limaye, N. R. Pavaskar, S. Ogale and M. Sastry, *Adv. Mater.*, 2003, **15**, 1273.
11 S. Feng and T. Bein, *Science*, 1994, **265**, 1839.
12 R. J. Park and F. C. Meldrum, *Adv. Mater.*, 2002, **14**, 1167.
13 C. Damle, A. Kumar, S. Bhagwat, S. R. Sainkar and M. Sastry, *Langmuir*, 2002, **18**, 6075.
14 S. A. Davis, M. Breulmann, K. H. Rhodes, B. Zhang and S. Mann, *Chem. Mater.*, 2001, **13**, 3218–3226.
15 N. H. de Leeuw, *J. Phys. Chem. B*, 2002, **106**, 5241–5249.
16 N. N. Aboukais, A. Boughriet, J. C. Fischer, M. Wartel, H. R. Langelin and A. Aboukais, *J. Chem. Soc., Faraday Trans.*, 1996, **92**, 3211.
17 J. L. Katz, M. R. Reick, R. E. Herzog and K. J. Parsiegla, *Langmuir*, 1993, **9**, 1423.
18 A. L. Braybrook, B. R. Heywood, R. A. Jackson and K. Pitt, *J. Cryst. Growth*, 2002, **243**, 336–334.
19 L. Pastero, E. Costa, M. Bruno, M. Rubbo, G. Sgualdino and D. Aquilano, *Cryst. Growth Des.*, 2004, **4**, 485–490.
20 S. Rajam and S. Mann, *J. Chem. Soc., Chem. Commun.*, 1990, 1789.
21 K. J. Davis, P. M. Dove and J. D. Yoreo, *Science*, 2000, **290**, 1134–1137.
22 Y. J. Han and J. Aizenberg, *J. Am. Chem. Soc.*, 2003, **125**, 4032–4033.
23 Y. Zhang and R. A. Dawe, *Chem. Geol.*, 2000, **163**, 129–138.
24 A. Sugawara and T. Kato, *Chem. Commun.*, 2000, 487–488.
25 F. C. Meldrum and S. T. Hyde, *J. Cryst. Growth*, 2001, **231**, 544–558.
26 E. Loste, R. M. Wilson, R. Seshadri and F. C. Meldrum, *J. Cryst. Growth*, 2003, **254**, 206–218.
27 G. Falini, S. Fermani, M. Gazzano and A. Ripamonti, *J. Mater. Chem.*, 1998, **8**, 1061–1065.
28 L. A. Gower and D. A. Tirell, *J. Cryst. Growth*, 1998, **191**, 153–160.
29 S. M. Stanley, J. B. Ries and L. A. Hardie, *Proc. Natl. Acad. Sci., U. S. A.*, 2002, **99**, 1523–1526.
30 S. Mandal, S. K. Arumugam, S. D. Adyanthaya, R. Pasricha and M. Sastry, *J. Mater. Chem.*, 2004, **14**, 43.
31 S. Mandal, S. K. Arumugam, R. Pasricha and M. Sastry, *Appl. Nano Sci.*, 2004(In Press).
32 T. Bala, S. K. Arumugam, R. Pasricha, B. L. V. Prasad and M. Sastry, *J. Mater. Chem.*, 2004, **14**, 1057.
33 T. Bala, S. D. Bhame, P. A. Joy, B. L. V. Prasad and M. Sastry, *J. Mater. Chem.*, 2004, **14**, 2941–2945.
34 B. D. Dong, J. J. Cilliers, R. J. Davey, J. Garside and E. T. Woodburn, *J. Am. Chem. Soc.*, 1998, **120**, 1625.
35 D. Rautaray, K. Sinha, S. ShivShankar, S. D. Adyanthaya and M. Sastry, *Chem. Mater.*, 2004, **16**, 1356–1361.
36 S. S. Shankar, U. S. Patil, B. L. V. Prasad and M. Sastry, *Langmuir*, 2004, **20**, 8853–8857.
37 K. Qin and D. K. Srivastava, *Biochemistry*, 1998, **37**, 3499.
38 M. M. Pierce, C. S. Raman and B. T. Nall, *Methods*, 1999, **19**, 213.
39 C. M. Barbieri, T. K. Li, S. Guo, G. Wang, A. J. Shallop, W. Pan, G. Yang, B. L. Gaffney, R. A. Jones and D. S. Pilch, *J. Am. Chem. Soc.*, 2003, **125**, 6469.
40 A. Kunne, M. Sieber, D. Meierhans and R. K. Allemann, *Biochemistry*, 1998, **37**, 4217.
41 M. R. Wenk and J. Seelig, *Biochemistry*, 1998, **37**, 3909.
42 H. Joshi, P. S. Shirude, V. Bansal, K. N. Ganesh and M. Sastry, *J. Phys. Chem. B*, 2004, **108**, 11535.
43 A. Gourishankar, S. Shukla, K. N. Ganesh and M. Sastry, *J. Am. Chem. Soc.*, 2004, **126**, 13186–13187.
44 The XRD patterns were indexed with reference to the unit cell of the aragonite structure (a = 4.959 Å, b = 7.968 Å, c = 5.741 Å; space group *Pmcn*, *ASTM* chart card no. 5-0453) and with reference to the unit cell of the calcite structure ($a = b$ = 4.989 Å, c = 17.062 Å, space group $D_{3D}{}^{6}$ – $R3c$, *ASTM* chart card no. 5-0586) from *ASTM* chart.
45 N. Nassrallah-Aboukais, A. Boughriet, J. Laureyns, A. Aboukais, J. C. Fischer, H. R. Langelin and M. Wartel, *Chem. Mater.*, 1998, **10**, 238–243.
46 G. Falini, S. Albeck, S. Weiner and L. Addadi, *Science*, 1996, **271**, 67–69.
47 R. M. Silverstein and F. X. Webster, *Spectrometric Identification of Organic Compounds*, *John Wiley & Sons, Inc.*, 6th edn., New York, 1998, p. 107.